

Redox-triggered chiroptical switching activity of ruthenium(III)-bis-(β-diketonato) complexes bearing a bipyridine-helicene ligand

Nidal Saleh, Nicolas Vanthuyne, Jacques Bonvoisin, Jochen Autschbach, Monika Srebro-Hooper, Jeanne Crassous

▶ **To cite this version:**

Nidal Saleh, Nicolas Vanthuyne, Jacques Bonvoisin, Jochen Autschbach, Monika Srebro-Hooper, et al.. Redox-triggered chiroptical switching activity of ruthenium(III)-bis-(β-diketonato) complexes bearing a bipyridine-helicene ligand. Chirality, 2018, 30 (5), pp.592-601. 10.1002/chir.22835 . hal-01728780

HAL Id: hal-01728780
https://hal.science/hal-01728780

Submitted on 5 Apr 2018

HAL is a multi-disciplinary open access archive for the deposit and dissemination of scientific research documents, whether they are published or not. The documents may come from teaching and research institutions in France or abroad, or from public or private research centers.

L'archive ouverte pluridisciplinaire **HAL**, est destinée au dépôt et à la diffusion de documents scientifiques de niveau recherche, publiés ou non, émanant des établissements d'enseignement et de recherche français ou étrangers, des laboratoires publics ou privés.

Redox-triggered chiroptical switching activity of ruthenium(III)-bis-(β-diketonato) complexes bearing a bipyridine-helicene ligand

Nidal Saleh,[a] Nicolas Vanthuyne,[b] Jacques Bonvoisin,[c] Jochen Autschbach,[d] Monika Srebro-Hooper,*[e] Jeanne Crassous*[a]

Abstract: Charged, electroactive bipyridine-helicene-ruthenium(III) complex [**4**]$^{\bullet+}$,PF_6^- has been prepared from 3-(2-pyridyl)-4-aza[6]helicene and a Ru-bis-(β-diketonato)-bis-acetonitrile precursor (β-diketonato: 2,2,6,6-tetramethyl-3,5-heptanedionato). Its chiroptical properties (electronic circular dichroism (ECD) and optical rotation) were studied both experimentally and theoretically and suggest the presence of two diastereoisomers, namely (*P*,*Δ*)- and (*P*,*Λ*)-[**4**]$^{\bullet+}$,PF_6^- (denoted jointly as (*P*,*Δ**)-[**4**]$^{\bullet+}$,PF_6^-) and their mirror-images (*M*,*Λ*)- and (*M*,*Δ*)-[**4**]$^{\bullet+}$,PF_6^- ((*M*,*Δ**)-[**4**]$^{\bullet+}$,PF_6^-). The electrochemical reduction of (*P*,*Δ**)-[**4**]$^{\bullet+}$,PF_6^- to neutral complex (*P*,*Δ**)-**4** was performed and revealed strong changes in the UV-vis and ECD spectra. A reversible redox-triggered chiroptical switching process was then achieved.

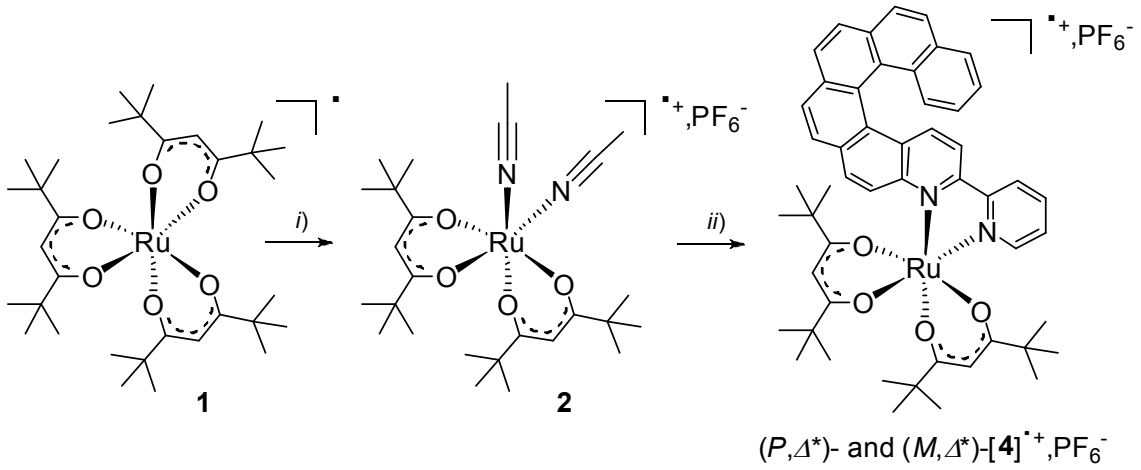
[a] *Dr. N. Saleh, Dr. J. Crassous, Institut des Sciences Chimiques de Rennes UMR 6226, CNRS Université de Rennes 1, Campus de Beaulieu, 35042 Rennes Cedex, France. E-mail: jeanne.crassous@univ-rennes1.fr*
[b] *Dr. N. Vanthuyne, Aix Marseille Université, Centrale Marseille, CNRS, iSm2 UMR 7313, 13397, Marseille, France*
[c] *Dr. J. Bonvoisin, CEMES, CNRS UPR 8011, Université de Toulouse, 29 Rue Jeanne Marvig, BP 94347, 31055 Toulouse Cedex 4, France*
[d] *Prof. J. Autschbach, Department of Chemistry, University at Buffalo, State University of New York, Buffalo, NY 14260, USA*
[e] *Dr. M. Srebro-Hooper, Faculty of Chemistry, Jagiellonian University, Gronostajowa 2, 30-387 Krakow, Poland. E-mail: srebro@chemia.uj.edu.pl*

Keywords: helicene, ruthenium, bipyridine, redox chiroptical switching, ECD spectroscopy, TDDFT calculations

Introduction

The inherent chirality of helicenes combined with their extended π-conjugation contribute to their appealing large-magnitude chiroptical properties, notably high values of optical rotation (OR) parameters, intense electronic circular dichroism (ECD) and vibrational circular dichroism (VCD) spectra, along with interesting (resonance) Raman optical activity ((R)ROA) and circularly polarized luminescence (CPL).[1] Combining organometallic and helicene chemistry via incorporation of an appropriate metallic ion within the helical backbone or via metal complexation and extension of the helicene π-electron system enables to tune and/or enhance the helicenes chiroptical properties and brings new interesting features and applications relying on the properties of the metal center.[2] One of the most appealing applications of such metal-helicenes is to use them as chiroptical molecular switches.[3] In this context, several classes of organometallic helicene-based complexes have been investigated in our groups, including i) ruthenium(II)-vinyl-[4,5] and iron(II)-ethynyl-carbo[6]helicenes[6] displaying redox-triggered switching of not only ECD and OR responses but also VCD and, in the case of Fe system, even RROA spectra, ii) cycloplatinated bipyridine-[6]helicene-based systems demonstrating acid/base-triggered tuning of ECD and CPL signals,[7] and iii) a bis-helicenic terpyridine derivative revealing an efficient absorption and emission switching activity through zinc(II) coordination/decoordination processes.[8]

In our aim to prepare novel families of stable and efficient redox-active chiroptical switches, the choice of an appropriate ligand that can stabilize the different redox states of a metallic ion is an important step. Herein, we describe the synthesis of stable octahedral Ru(III) complexes ([**4**]$^{\bullet+}$,PF_6^-, Scheme 1) bearing a helicenic bipyridine and two tmhd (tmhd: 2,2,6,6-tetramethyl-3,5-heptanedionato) ligands. Indeed, bipyridines are widely used ligands that can stabilize metal centers through their strong σ-donating and weak π-back-bonding character,[9,10] while π-conjugated electron-rich β-diketonate ions, such as acac or tmhd, are known to support mixed-ligand Ru complexes, and, due to their non-innocent behavior, can consequently give access to stable compounds of electroactive properties.[11-14] These novel chiral propeller-like systems have been characterized via electrochemistry studies, UV-vis and ECD spectroscopy, and first-principles calculations. Spectroelectrochemical studies have demonstrated that the complexes reveal an efficient redox-triggered chiroptical switching, thus yielding a new example of organometallic helicene-based switch.



SCHEME 1. Preparation of the mixed-ligand Ru(III) complex $[\mathbf{4}]^{\bullet+},PF_6^-$. *i*) conc. H_2SO_4, aq. NH_4PF_6, CH_3CN, reflux,1 hr, 90%; *ii*) bipyridine-carbo[6]helicene (*rac*-, *P*- or *M*-**3**), DMF, 140°C, 3 hrs, 85%.

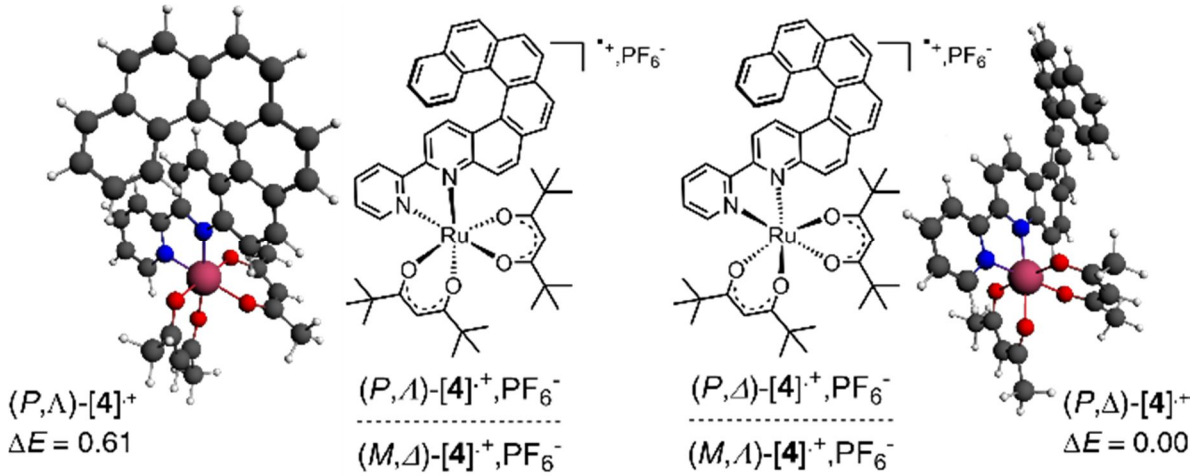


FIGURE 1. Chemical structures of a diastereomeric pair (*P*,*Λ*)- and (*P*,*Δ*)-$[\mathbf{4}]^{\bullet+},PF_6^-$ (denoted as (*P*,*Δ**)-$[\mathbf{4}]^{\bullet+},PF_6^-$) along with the corresponding optimized (BP/SV(P) with continuum solvent model for CH_2Cl_2) molecular structures of $[\mathbf{4}]^{\bullet+}$ and their relative energies, ΔE in kcal mol^{-1} (see also SI).

Materials and Methods

General. Experiments were performed using standard Schlenk techniques. Starting materials were purchased from Sigma Aldrich. Column chromatography purifications were performed in air over silica gel (Merck Geduran 60, 0.063–0.200 mm). Elemental analyses were performed by the CRMPO (*Centre régional de mesures physiques de l'Ouest*), Université de Rennes 1. Circular dichroism (in M^{-1} cm^{-1}) was measured on a Jasco J-815 Circular Dichroism Spectrometer (IFR140 facility - Biosit platform Université de Rennes 1). The target complex was synthesized according to Scheme 1. The starting precursors $Ru(tmhd)_3$ **1** and $[Ru(tmhd)_2(CH_3CN)_2]^{\bullet+},PF_6^-$ **2** and racemic and enantiopure bipyridine-helicene (*rac*-, *P*- or *M*-**3**) were prepared according to literature procedures.[7,15]

Synthesis of racemic $[\mathbf{4}]^{\bullet+}PF_6^-$. To a solution of **2** (20 mg, 0.03 mmol) in DMF (3 mL) was added a solution of *rac*-**3** (12 mg, 0.03 mmol) in DMF (3 mL). The mixture was then heated at 140°C for 3 hrs. Then the solvent was stripped off and the crude compound was purified by silica gel chromatography (THF as the eluent), yielding *rac*-$[\mathbf{4}]^{\bullet+},PF_6^-$ as a brown solid (25 mg, 85%).

Anal. calcd. for $C_{52}H_{62}F_6N_2O_4PRu$: C, 60.93; H, 6.10; found: C 60.57, H 6.56.
The same procedure was applied to enantiopure *P*- and *M*-**3**[7,16,17] to yield (*P*,Δ*)- and (*M*,Δ*)-[**4**]$^{\bullet+}$,PF_6^-, respectively. Δ* refers to either Δ or Λ ruthenium stereochemistry.

Computational details. All calculations were carried out with the Turbomole package (TM6.6),[18,19,20] using Kohn-Sham (KS) density functional theory (KST, or DFT) and its time-dependent variant (TDKS, or TDDFT).[21,22] Geometry optimizations were performed for tmhd/bipyridine-helicene complexes of Ru(III) ((*P*,Δ)-[**4**]$^{\bullet+}$ and (*P*,Λ)-[**4**]$^{\bullet+}$ in a spin-doublet d^5 electronic configuration, Figure 1) and of Ru(II) ((*P*,Δ)-**4** and (*P*,Λ)-**4** in a closed-shell d^6 configuration). Corresponding truncated models, in which tmhd ligands were replaced by acac (acac = pentane-2,4-dionate) anions, are labelled as [**4**$^{\mathbf{Me}}$]$^{\bullet+}$ and **4**$^{\mathbf{Me}}$. The optimizations employed the BP[23,24,25] exchange-correlation functional. The electron spin density, $\Delta\rho = \rho_\alpha - \rho_\beta$, in [**4**]$^{\bullet+}$ and [**4**$^{\mathbf{Me}}$]$^{\bullet+}$ was analyzed using the B3LYP[26,27,28] functional in its default TM6.6 parametrization. The truncation of the β-diketonato ligands was found to have only a slight effect on the energetic difference between (*P*,Δ)/(*M*,Λ) and (*P*,Λ)/(*M*,Δ) stereoisomers and seems not to affect the electronic structure of both systems (see Figures S1 and S2 in the Supporting Information, SI). Consequently, the subsequent UV-vis and ECD calculations and further analysis were performed only for the model systems. The corresponding TDDFT linear response calculations of the sodium-D line (λ = 589.3 nm) ORs, singlet excitation energies, as well as the associated dipole and rotatory strengths were carried out with three global hybrid functionals with increasing fractions of exact exchange (in parentheses): B3LYP (20%), PBE0 (25%),[29] and BHLYP (50%).[30] Simulated spectra for the bipyridine-helicene ligand **3** were taken from Reference 7.

In all aforementioned computations a split-valence basis set with one set of polarization functions for non-hydrogen atoms, SV(P),[31,32,33] was employed. Scalar relativistic effects for the Ru atoms were treated implicitly by the use of a 60-electron relativistic effective core potential (ECP).[34] Solvent effects (dichloromethane, DCM, ε = 8.9) were included in the calculations via the conductor-like screening model (COSMO) with the default parameters of the TM6.6/COSMO implementation.[35,36] No significant changes in the results are expected for dichloroethane (DCE) solvent model because its dielectric constant (ε = 10.66) is similar to DCM, as previously noticed in Reference 11.

The TDDFT calculations reported here cover from 200 to 440 (depending on the functional) lowest singlet excited states to assure that all transitions with a significant rotatory strength in the experimentally observed energy range are included. The simulated absorption and ECD spectra shown are the sums of Gaussian functions centered at the vertical excitation energies and scaled using the calculated dipole and rotatory strengths, with a parameter of σ = 0.2 eV applied for the root mean square width.[37] A comparison of measured and simulated ECD spectra (see Figures S3 and S4) shows that all three functionals demonstrate, in general, very similar performance in reproducing the experimentally observed spectral trends, especially when considering a 50:50 diastereomeric mixture of (*P*,Δ)- and (*P*,Λ)-[**4**]$^{\bullet+}$ / (*P*,Δ)- and (*P*,Λ)-**4** with B3LYP / BHLYP leading to the most red-shifted / blue-shifted spectra. As the most consistent ECD results for individual epimers along with the most reliable OR values (Table S5) were obtained with the BHLYP functional, the spectra were assigned based on these calculations.

Results and Discussion

SYNTHESIS

The synthesis of [**4**]$^{\bullet+}$,PF_6^- complexes is depicted in Scheme 1. Commercially available Ru(tmhd)$_3$ **1** is characterized by its volatility, good thermal and atmospheric stability as well as its solubility in common organic solvents.[38,39] Reacting it with acetonitrile in the presence of sulfuric acid, according to a literature procedure,[15] yielded mixed-ligand [Ru(tmhd)$_2$(CH_3CN)$_2$]$^{\bullet+}$,PF_6^- **2**. The labile CH_3CN ligands can then be easily replaced, thus allowing to prepare a wide range of stable mixed-ligand Ru(III) complexes.[11-15] Hence, the reaction between **2** and racemic bipyridine-carbo[6]helicene *rac*-**3** in refluxing toluene, resulted in the formation of the mononuclear cationic Ru(III) complex [**4**]$^{\bullet+}$,PF_6^- as a brown precipitate that was obtained in 85% yield after purification over silica gel column chromatography. The [**4**]$^{\bullet+}$,PF_6^- compound displayed a broad and unresolved ^{1}H NMR spectrum, probably due to its paramagnetic and diastereomeric character. The complex [**4**]$^{\bullet+}$,PF_6^- shows an excellent atmospheric stability as is usually observed in such types of compounds.[38,39] Furthermore, the stable complexes (*P*,Δ*)- and (*M*,Δ*)-[**4**]$^{\bullet+}$,PF_6^- (where Δ* refers to either Δ_{Ru} or Λ_{Ru} epimers) were obtained by reacting the precursor **2** with enantiopure *P*- and *M*-**3**. Indeed, due to the presence of two stereogenic elements, namely the *P* and *M* helices and the Δ and Λ octahedral Ru center, a set of diastereomeric pairs are expected, *i.e.* (*P*,Λ)-/(*M*,Δ)-[**4**]$^{\bullet+}$,PF_6^- and (*P*,Δ)-/(*M*,Λ)-[**4**]$^{\bullet+}$,PF_6^- (Figure 1). According to the DFT calculations (see Computational details), (*P*,Λ)-[**4**]$^{\bullet+}$ and (*P*,Δ)-[**4**]$^{\bullet+}$ demonstrate comparable energy values, with a slight preference of the latter (by 0.6 – 0.9 kcal·mol^{-1}, depending on the method used, Figure 1 and SI), indicating that on thermodynamic grounds, [**4**]$^{\bullet+}$ may indeed exist as a mixture of both diastereomers. However, all our attempts to separate these two epimers by HPLC failed, mainly due to system stability issues under the HPLC conditions.

UV-VIS AND CHIROPTICAL PROPERTIES

Although our attempts to obtain enantiopure (*P*,Λ)-/(*M*,Δ)- and (*P*,Δ)-/(*M*,Λ)-[**4**]$^{\bullet+}$,PF_6^- samples were unsuccessful (*vide supra*), we examined UV-vis and chiroptical properties (OR values and ECD spectra) for the diastereomeric mixture of both complexes, *i.e.* (*P*,Δ*) and (*M*,Δ*)-[**4**]$^{\bullet+}$,PF_6^-. The UV-vis absorption spectrum of [**4**]$^{\bullet+}$,PF_6^- measured in dichloromethane (CH_2Cl_2 = DCM) is shown in Figure 2a. It displays one intense absorption band (ε > 50 000 M^{-1} cm^{-1}) at 275 nm and two bands of moderate intensity around 310 and 340 nm, which are similar to the starting ligand **3**,[7] along with new broad, weaker bands centered around 410 and 510 nm (*vide infra*). As far as chiroptical properties are concerned (*P*,Δ*)- and (*M*,Δ*)-[**4**]$^{\bullet+}$,PF_6^- complexes demonstrate the expected opposite-sign molar and specific rotation values (for instance for the *P* enantiomer: $[\alpha]_D^{23}$ = +1040 degree [dm (g cm^{-3})]$^{-1}$, $[\Phi]_D^{23}$ = +10600 degree cm^2 dmol^{-1}, the latter is comparable to *P*-**3**:[7] +12000 degree cm^2 dmol^{-1}) and mirror-image ECD spectra (Figure 2b). The experimental ECD of (*P*,Δ*)-[**4**]$^{\bullet+}$,PF_6^-

shows three intense bands: i) a strong negative band at 270 nm ($\Delta\varepsilon$ = -104 M^{-1} cm^{-1}), and ii) two positive bands of moderate intensity at 335 nm ($\Delta\varepsilon$ = +66 M^{-1} cm^{-1}) and 370 nm ($\Delta\varepsilon$ = +78 M^{-1} cm^{-1}), which seem to correspond to the ECD-active bands observed for *P*-**3** (Figure 2b),[7] but with decreased intensity likely due to effects from the Ru center (*vide infra*). In addition, a new positive band at around 420 nm ($\Delta\varepsilon$ = +30 M^{-1} cm^{-1}) and a very weak negative band at 497 nm ($\Delta\varepsilon$ = -3 M^{-1} cm^{-1}) are also present in the ECD spectrum of (*P*,*Δ**)-[**4**]$^{\bullet+}$,PF_6^-.

Calculations (TDDFT BHLYP/SV(P) with a continuum solvent model for DCM) performed for the truncated systems [$\mathbf{4^{Me}}$]$^{\bullet+}$ correctly reproduce the experimental data. As can be seen from Figure 3, both (*P*,*Λ*)-[$\mathbf{4^{Me}}$]$^{\bullet+}$ and (*P*,*Δ*)-[$\mathbf{4^{Me}}$]$^{\bullet+}$ reveal very similar overall UV-vis and ECD spectral envelopes that match well the experimental spectra for their assumed 50:50 diastereomeric ((*P*,*Δ**)) mixture. Similarly, the calculated molar rotation values ((*P*,*Λ*)-[$\mathbf{4^{Me}}$]$^{\bullet+}$: +17356, (*P*,*Δ*)-[$\mathbf{4^{Me}}$]$^{\bullet+}$: +10701, (*P*,*Δ**)-[$\mathbf{4^{Me}}$]$^{\bullet+}$: +14028 degree cm^2 $dmol^{-1}$) agree with the experiment in a satisfactory manner. The similar chiroptical properties computed for both (*P*,*Λ*) and (*P*,*Δ*) epimers imply that the effect of the bipyridine-helicene stereochemistry surpasses that from the ruthenium center. To gain insight into experimentally observed spectral features, a detailed analysis of the electronic structure of the [$\mathbf{4^{Me}}$]$^{\bullet+}$ complexes and an assignment of their electronic spectra was performed.

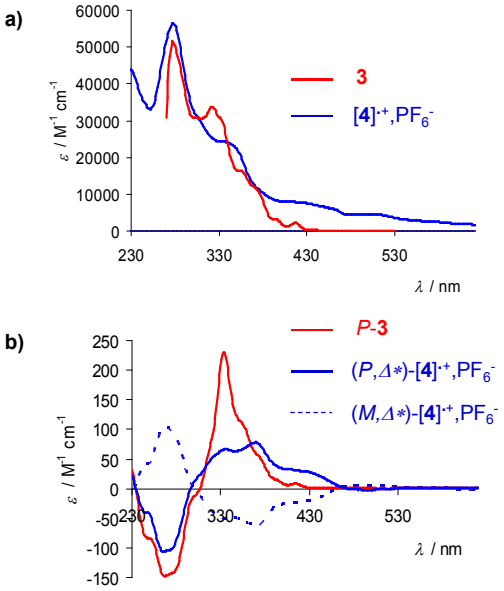


FIGURE 2. a) UV-vis absorption spectrum of ligand **3**[7] and complex [**4**]$^{\bullet+}$,PF_6^- along with b) ECD spectra of *P*-**3**,[7] (*P*,*Δ**)- and (*M*,*Δ**)-[**4**]$^{\bullet+}$,PF_6^- (CH_2Cl_2, *C* 5 10^{-5} M).

Both [$\mathbf{4^{Me}}$]$^{\bullet+}$ diastereomers demonstrate very similar orbital isosurfaces and orbital energies of the frontier MOs (see Figure 4 top and SI). The plot of the electron spin density of the low-spin d^5 configuration clearly shows that the unpaired electron is not only localized on the ruthenium metal center but, to some degree, also spread out over the β-diketonato π-systems in line with the π-donating character and non-innocent behavior of these ligands.[11] The highest-energy occupied MOs (165-167(α) and 164-166(β)) are centered at the (bipyridine-)helicene ligand and reveal negligible π-conjugation with the metal *d* orbitals. Note however that the Ru orbital contributions to the frontier MOs may be somewhat underestimated as the BHLYP functional tends to lead to unphysically strong electron localization (see also SI).[40] At lower energy are non-bonding Ru d_π orbitals (formally t_{2g} *d* orbitals of local π-symmetry with respect to the metal-ligands bonds, *i.e.* d_{xy}, d_{yx}, d_{xz}) in out-of-phase combinations with β-diketonate orbitals.[11] The visual comparison of the isosurface plots in the α- and β-spin MO sets establishes MO164(α) as the (unpaired) singly occupied MO, SOMO, and the lowest-energy unoccupied MO167(β) as its opposite-spin partner orbital representing an 'electron hole' in the β-spin density. The square of both orbitals resembles the calculated spin density distribution although clear signatues of relaxation and spin polarization processes can also be seen in the spin density. The higher-energy unoccupied MOs are bipyridine-helicene-centered π* orbitals that are localized predominantly on the (Ru-)bipyridine-N^N' fragment (MO168(α,β)) or on the central parts of the ligand structure (MO169(α,β)).

Analysis of selected dominant excitations of (*P*,*Λ*)-[$\mathbf{4^{Me}}$]$^{\bullet+}$ and (*P*,*Δ*)-[$\mathbf{4^{Me}}$]$^{\bullet+}$ in terms of individual MO pairs (see SI for the full set of data) indicates that the low-energy (ca. 400-500 nm) band of the [**4**]$^{\bullet+}$ UV-vis absorption spectrum, which corresponds to the low-energy tail of the first positive ECD band, is caused by excitation no. 14 calculated at ca. 390 nm and assigned as π-to-π* intra-ligand (IL) / ligand-to-metal (LM) charge transfer (CT) involving the α- and β-occupied helicene-centered MO167(α) and MO166(β), and the unoccupied bipyridine-N^N'-centered MO168(α) and Ru-bipyridine-N^N'-centered MO167(β) ('electron hole') and MO168(β), respectively. The main positive intense band of [**4**]$^{\bullet+}$ experimentally observed around 350 nm originates from excitation no. 29 (calculated at 330 nm) that also corresponds mainly to π-to-π* transitions localized in the π-conjugated system of the Ru(d_π)-bipyridine-

helicene moiety of CT-like (MO166(β)-to-MO169(β) and MO167(α)-to-MO169(α)) and LM CT (MO165(β)-to-MO168(β)) character. Ruthenium-centered excitations (*e.g.* nos. 19, 20, 23) exhibit generally much smaller intensity, often cancelling each other in the ECD spectrum, and, as expected, revealing opposite rotatory strengths for (*P,Λ*)-[**4**$^{\mathbf{Me}}$]$^{\bullet+}$ and (*P,Δ*)-[**4**$^{\mathbf{Me}}$]$^{\bullet+}$ epimers. The analysis clearly highlights the impact of the stereochemistry of bipyridine-helicene ligand on the observed properties of its β-diketonato-Ru complexes, as it dominates over the metal configuration. Furthermore, based on the experimental ECD spectra, it can be noted that although the Ru center has a mixed *Δ*/*Λ* stereochemistry, it is able to sense its chiral environment, thus displaying a net Cotton effect around 500 nm (negative for the *P* helical ligand and positive for *M*).

UV-VIS/NIR SPECTROELECTROCHEMISTRY

Cyclic voltammetry (CV) was recorded in DCM under an argon atmosphere with 0.1 M tetrabutylammonium hexafluorophosphate (TBAH). The $E_{1/2}$ potential was determined from the average of the anodic and cathodic peak potentials for reversible wave. The cyclic voltammogram of the complex [**4**]$^{\bullet+}$,PF_6^- revealed only one reversible wave in reduction at -0.328 V *vs.* ferrocene/ferrocenium (Fc/Fc^+) standard as shown in Figure 5, corresponding to the creation of a neutral complex **4** (Scheme 2). Compared to classical $Ru(acac)_3$ derivatives,[11] this wave is shifted to the anodic potentials due to the substitution of one anionic "acac" ligand by a neutral "pyridine" one.

The one-electron reduction process of [**4**]$^{\bullet+}$,PF_6 → **4** (Scheme 2) was then monitored by UV/vis/NIR spectroscopy in an optically transparent thin-layer electrochemical (OTTLE) cell ($C_2H_4Cl_2$ = DCE / NBu_4PF_6, 0.2 M) upon reduction at -0.6 V *vs.* a Pt pseudo-potential electrode. The UV/vis/NIR spectro-electrochemical study of the reduction process revealed an increase of the high energy bands ~ 275 nm, several modifications with isosbestic points between 290-510 nm, and the appearance of a lower-energy broad absorption band centered at ~670 nm of moderate intensity (ε ~ 6 10^3 M^{-1} cm^{-1}) tailing down to 850 nm (Figure 6a). The reverse oxidation process was also performed by applying a potential at +0.6 V *vs.* a Pt pseudo-potential electrode and full reversibility was observed (*vide infra*).

These differences in the spectroelectrochemical electronic absorption spectroscopy were also reflected in the corresponding ECD spectra of (*P,Δ**)- and (*M,Δ**)-[**4**]$^{\bullet+}$,PF_6^- (Figure 6b). Indeed, the reduction of (*P,Δ**)-[**4**]$^{\bullet+}$,PF_6^- to (*P,Δ**)-**4** resulted in a significant increase of the negative ECD-active band at 270 nm ($\Delta\varepsilon$ = -128 M^{-1} cm^{-1}, $\Delta(\Delta\varepsilon)$ = -36 M^{-1} cm^{-1}) accompanied by its 10 nm blue-shift and of the positive band at 340 nm ($\Delta\varepsilon$ = +129 M^{-1} cm^{-1}, $\Delta(\Delta\varepsilon)$ = +79 M^{-1} cm^{-1}). Moreover, the decrease of the positive band at 430 nm was complemented by a slight increase in intensity of the negative band at 500 nm ($\Delta\varepsilon$ = -7 M^{-1} cm^{-1}, $\Delta(\Delta\varepsilon)$ = -4 M^{-1} cm^{-1}) and appearance of a very weak positive and negative bands respectively around 605 nm ($\Delta\varepsilon$ = +2 M^{-1} cm^{-1}) and in the NIR region around 750 nm ($\Delta\varepsilon$ = -3 M^{-1} cm^{-1}). Note that the ECD spectrum of Ru(II) complex **4** resembles that of the starting ligand **3** (see Figure 7) but with an additional fingerprint (negative-positive-negative progression from 430 to 900 nm). Apart from a blue-shift, the calculations reproduce the general experimental trends for **4** *vs.* [**4**]$^{\bullet+}$,PF_6^- and **3** satisfactoryly (see Figure 3) and allow us to link them to the changes in the electronic structure of the complexes occurring upon the reduction process.

As illustrated in Figure 4 bottom (see also SI), reduction of the Ru(III) [**4**$^{\mathbf{Me}}$]$^{\bullet+}$ to the Ru(II) **4**$^{\mathbf{Me}}$ leads to the closed-shell d^6 electronic configuration with substantially destabilized occupied d_π MOs (165-167) at higher energy than the occupied (bipyridine-)helicene-centered orbitals (163-164, *vide supra*). The frontier unoccupied MOs (168-169) in **4**$^{\mathbf{Me}}$ remain of predominant π*-bipyridine-helicene character. MO-pair analysis of the intense excitations of (*P,Λ*)-**4**$^{\mathbf{Me}}$ and (*P,Δ*)-**4**$^{\mathbf{Me}}$ shows, in line with results obtained for pure diketonato ruthenium complexes,[11] that the ECD changes for **4** *vs.* [**4**]$^{\bullet+}$,PF_6^- are directly caused by the disappearing contributions from the β-spin 'electron hole' d_π MO and the energetic destabilization of the Ru orbitals due to the increased electron repulsion in the *d* shell. Namely, unlike for (*P,Δ**)-[**4**$^{\mathbf{Me}}$]$^{\bullet+}$, the low-energy part of the (*P,Δ**)-**4**$^{\mathbf{Me}}$ spectrum (between 380-580 nm) is dominated by metal-to-ligand (ML) CT excitations with sizable, mainly negative, rotatory strengths (see *e.g.* excitations nos. 2 (calculated at ca. 482 nm), 3 (467 nm), 5 (375 nm)) that involve transitions from non-bonding Ru(d_π)-centered MO165-167 to the bipyridine-N^N'-centered MO168. The negative-positive-negative progression observed experimentally between 430-900 nm in the ECD spectrum of (*P,Δ**)-**4** is reproduced by the BHLYP calculations only partially by the presence of negative intensity around 480 nm. This may be a result of approximations in the functional (this part of the spectrum is sensitive to the choice of functional, see SI) or due to vibronic effects, which were not modeled. An increase in the intensity of the ECD band at around 350 nm occurring upon reduction of [**4**]$^{\bullet+}$,PF_6^- can be rationalized as the effect of i) appearance of additional intense excitations of predominantly mixed π-to-π* helicene → bipyridine-N^N' IL and Ru(d_π) → helicene ML CT character (*e.g.* excitation no. 9, calculated at ca. 347 nm), and ii) change in the character of the underlying dominant electronic excitation (no. 13, calculated at 320 nm) that reveals a stronger involvement of helicene π-orbitals and consequently larger rotatory strength. As in the case of [**4**$^{\mathbf{Me}}$]$^{\bullet+}$, ruthenium-centered excitations (*e.g.* no. 11) exhibit generally smaller intensity and opposite rotatory strengths for the opposite metal configurations.

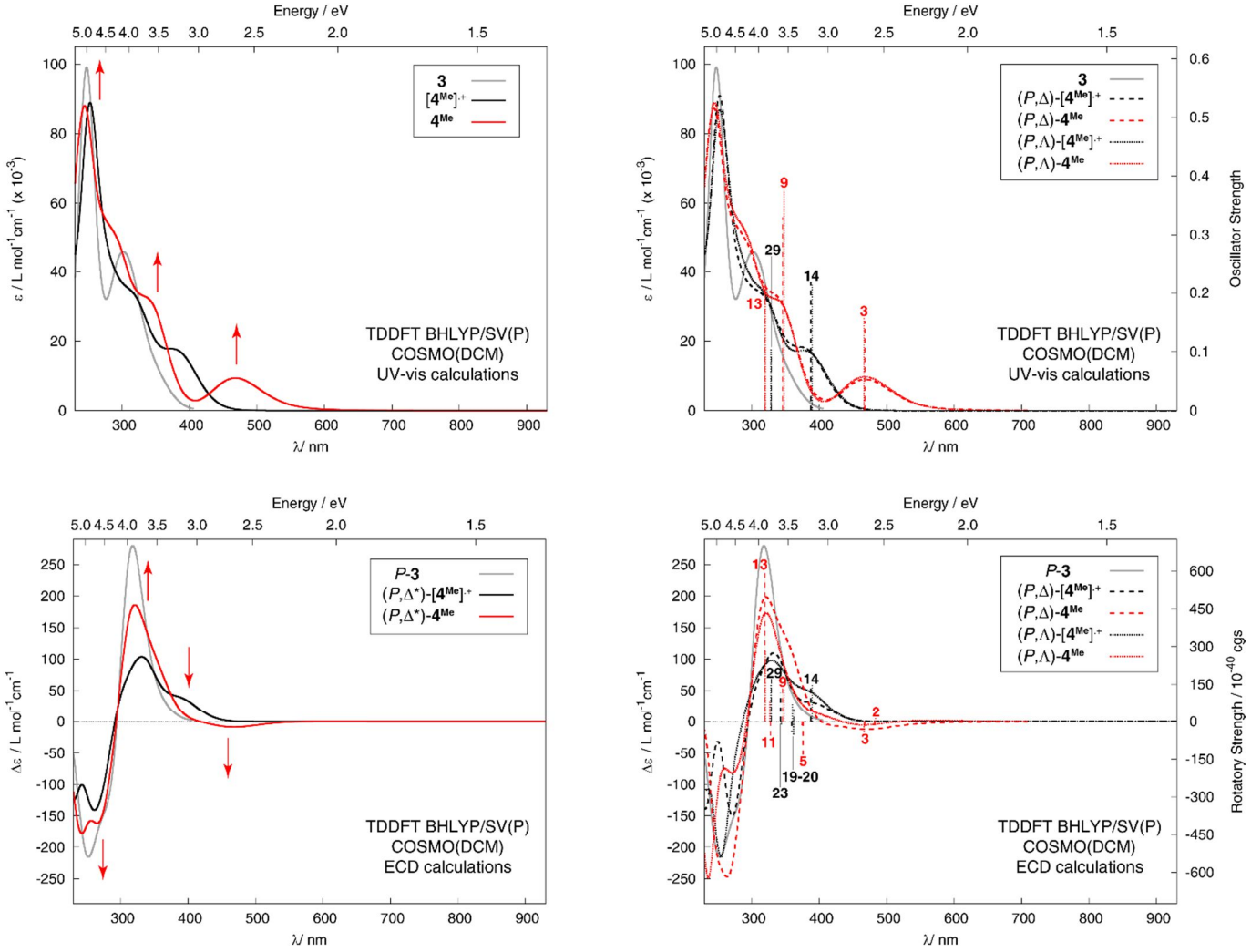


FIGURE 3. Comparison of the simulated (BHLYP) UV-vis (top) and ECD (bottom) spectra of (*P,Δ*)-/(*P,Λ*)-[**4**$^{\mathbf{Me}}$]$^{\bullet+}$, (*P,Δ*)-/(*P,Λ*)-**4**$^{\mathbf{Me}}$, their assumed 50:50 diastereomeric mixtures, (*P,Δ**)-[**4**$^{\mathbf{Me}}$]$^{\bullet+}$ and (*P,Δ**)-**4**$^{\mathbf{Me}}$, and the bipyridine-[6]helicene **3**. No spectral shift has been applied. Calculated excitation energies and rotatory strengths indicated as 'stick' spectra. Numbered excitations correspond to those analyzed in detail (see also SI). Arrows indicate changes in the spectra due to the redox processes.

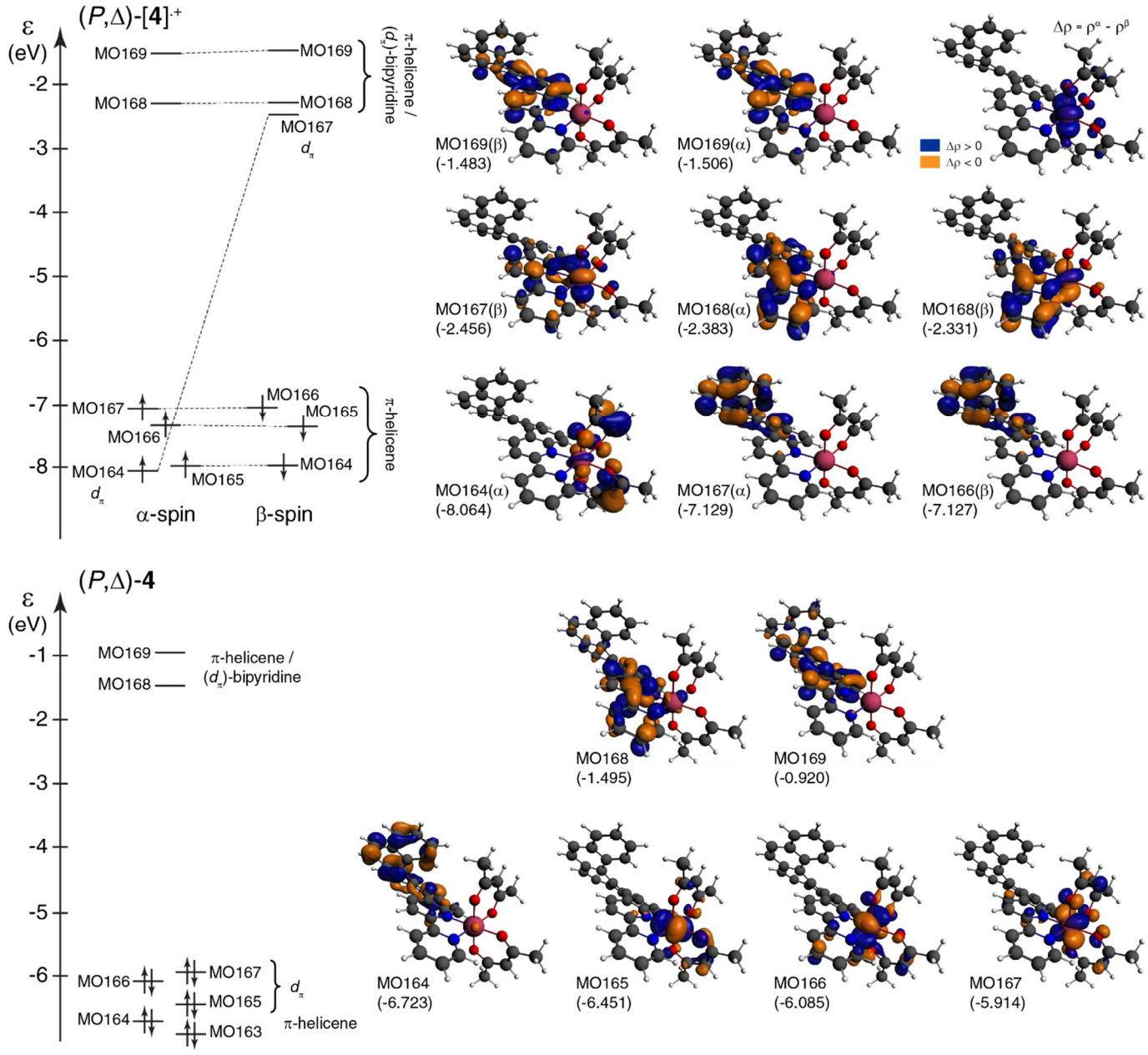


FIGURE 4. (Left:) BHLYP/SV(P) MO energy levels for (*P,Δ*)-[**4**^{Me}]$^{\bullet+}$ (separately for α-spin (spin-up) and β-spin (spin-down) orbitals) and for (*P,Δ*)-**4**^{Me} along with (right:) isosurfaces (±0.04 au) of selected frontier MOs and their corresponding orbital energies ε, in eV (in parentheses). For (*P,Δ*)-[**4**^{Me}]$^{\bullet+}$ the isosurface (±0.003 au) of the electron spin density $\Delta\rho$ is also shown in the right top corner. See also SI.

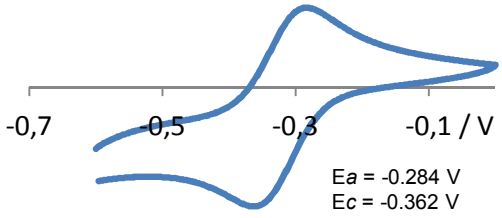
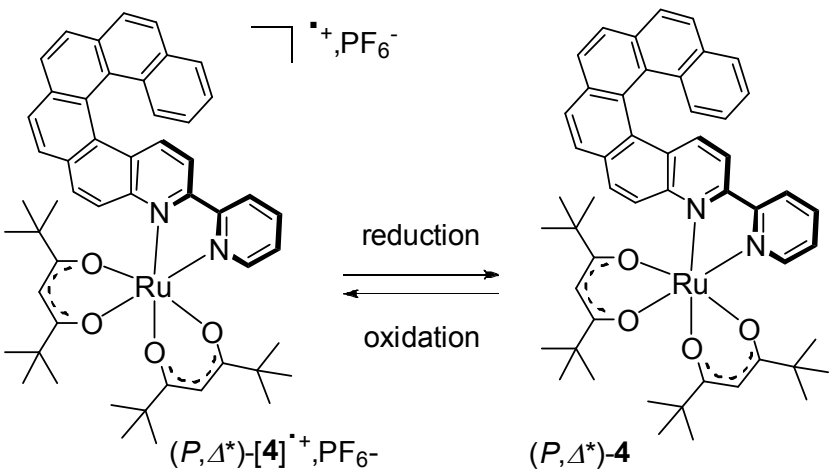


FIGURE 5. Cyclic voltammetry of [**4**]$^{\bullet+}$,PF_6^- in CH_2Cl_2 and TBAH (0.1 M) *vs.* Fc/Fc^+.



SCHEME 2. Electrochemical reduction ↔ oxidation process of Ru-bipyridine-[6]helicene β-diketonato complex (*P*,Δ*)-[**4**]$^{\bullet+}$,PF_6^- ↔ (*P*,Δ*)-**4**.

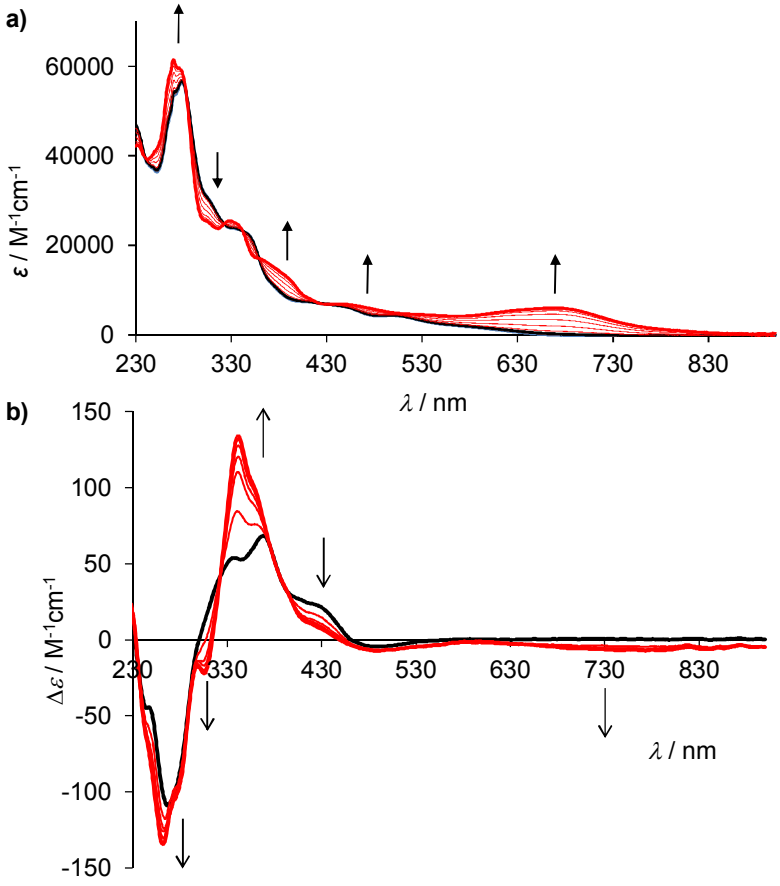


FIGURE 6. Spectroelectrochemical a) UV-vis/NIR and b) ECD studies of the reduction process (*P*,Δ*)-[**4**]$^{\bullet+}$,PF_6^- (black) → (*P*,Δ*)-**4** (red). Arrows indicate changes in the spectra due to the redox processes.

As the comparison between the ECD spectra of Ru(II) and Ru(III) species shows remarkable changes in the chiroptical properties, the electrochemical reversibility of [**4**]$^{\bullet+}$,PF_6^- was then exploited to explore the capability of this system to act as a chiroptical switch. For (*M*,*Δ**)-[**4**]$^{\bullet+}$,PF_6^- the ECD effect, *Δ*(*Δε*) at 750 nm is weak (+3 M^{-1} cm^{-1}), but it is attributed to the appearance of a new band and thus its reversibility with (*M*,*Δ**)-[**4**]$^{\bullet+}$,PF_6^- ↔ (*M*,*Δ**)-**4** interconversion may be an indication of an ON/OFF chiroptical switching. Indeed, (*M*,*Δ**)-[**4**]$^{\bullet+}$,PF_6 can be reduced and oxidized for several cycles (14 cycles / hr) accompanied by a reversible modulation of the ECD signal upon applying potential steps between −0.6 and 0 V of a DCE solution (0.2 M, *n*-Bu_4PF_6) in an electrochemical cell as shown in Figure 8. Consequently, the novel bis-(β-diketonato) Ru complexes bearing the bipyridine-helicene ligand showed an efficient reversibility and interesting stability for more than one hour, thus yielding a new example of redox-triggered chiroptical switch based on an organometallic helicene.

Conclusion

Grafting a Ru-bis-(*β*-diketonato) moiety onto a helicenic bipyridine ligand can lead to a new type of organometallic helicene derivative [(*P*,*Δ**)- and (*M*,*Δ**)-[**4**]$^{\bullet+}$,PF_6^-]. Noteworthy, even if the *Δ*/*Λ* stereochemistry at the octahedral the Ru center is not fixed, the Ru can sense the *M* / *P* helicity of the π-helical ligand, thus giving a positive / negative ECD-active band around 500 nm. Furthermore, the (*P*,*Δ**)-[**4**]$^{\bullet+}$,PF_6^- → (*P*,*Δ**)-**4** reduction process yielded significant modifications in the UV-vis and ECD spectra originating, as revealed by first-principles calculations, from the changes in the orbital energies of the complex, and their occupations, upon reduction. Finally, due to the efficient and reversible redox process and the strong ECD changes, this system may function as a redox-triggered chiroptical switch.

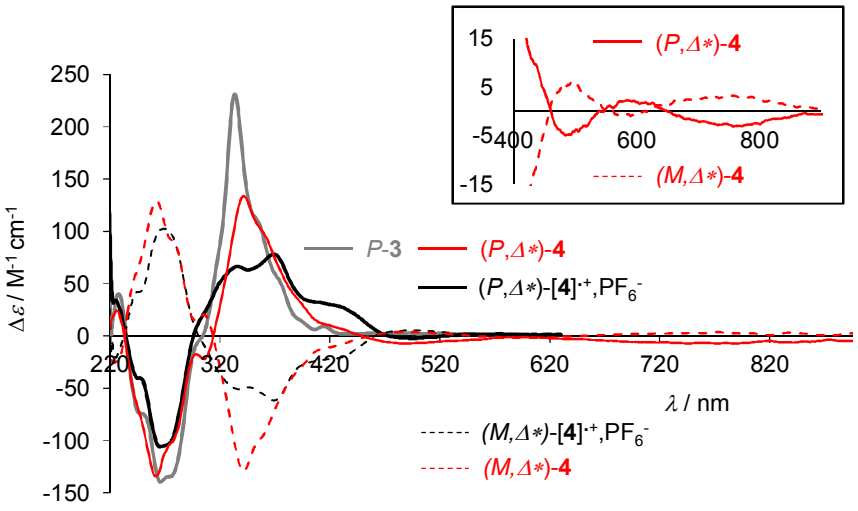


FIGURE 7. Comparison of the experimental ECD spectra of bipyridine-helicene ligand *P*-**3**[7] and of its (*P*,*Δ**) and (*M*,*Δ**) diketonato Ru(III) ([**4**]$^{\bullet+}$,PF_6^-, black) and Ru(II) (**4**, red) complexes.

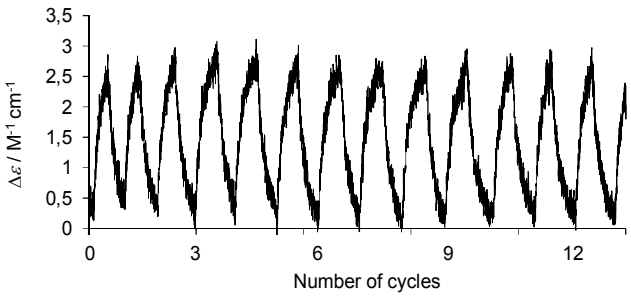


FIGURE 8. Redox-triggered chiroptical switch of (*M*,*Δ**)-[**4**]$^{\bullet+}$,PF_6^- ↔ (*M*,*Δ**)-**4** at 750 nm.

Acknowledgements

We thank the Ministère de l'Education Nationale, de la Recherche et de la Technologie, the Centre National de la Recherche Scientifique (CNRS) and the University of Rennes 1. This work was supported by the ANR (grants n° ANR 2010 BLAN 724 3) and the Chirafun CNRS network. M.S.-H. acknowledges the young researchers' T-subsidy from the Ministry of Science and Higher Education in Poland. J.A. acknowledges NSF Grant CHE-1560881. Christine Viala (CEMES) is aknowledged for technical and chemical assistance.

Supporting information

Additional supporting information may be found in the online version of this article at the publisher's website.

REFERENCES AND NOTES

1. See recent monography: Shen Y, Chen, CF. *Helicenes Chemistry: From Synthesis to Applications*, Springer, Berlin, 2017.
2. Saleh N, Shen C, Crassous J. Helicene-based transition metal complexes: synthesis, properties and applications. *Chem. Sci.* 2014;5:3680-3694.
3. Isla H, Crassous J. Helicene-based chiroptical switches. *C R Chimie*. 2016;19:39-49.
4. Anger E, Srebro M, Vanthuyne N, Toupet L, Rigaut S, Roussel C, Autschbach J, Crassous J, Reau R. Ruthenium-vinylhelicenes: remote metal-based enhancement and redox switching of the chiroptical properties of a helicene core. *J Am Chem Soc*. 2012;134:15628-15631.
5. Srebro M, Anger E, Moore B II, Vanthuyne N, Roussel C, Reau R, Autschbach J, Crassous J. Ruthenium-grafted vinylhelicenes: chiroptical properties and redox switching. *Chem Eur J*. 2015;21:17100-17115.
6. Shen C, Loas G, Srebro-Hooper M, Vanthuyne N, Toupet L, Cador O, Paul F, López Navarrete JT, Ramírez FJ, Nieto-Ortega B, Casado J, Autschbach J, Vallet M, Crassous J. Iron alkynyl helicenes: redox-triggered chiroptical tuning in the IR and near-IR spectral regions and suitable for telecommunications applications. *Angew Chem Int Ed.* 2016;55:8062-8066.
7. Saleh N, Moore B II, Srebro M, Vanthuyne N, Toupet L, Williams JAG, Roussel C, Deol KK, Muller G, Autschbach J, Crassous J. Acid/base-triggered switching of circularly polarized luminescence and electronic circular dichroism in organic and organometallic helicenes. *Chem Eur J*. 2015;21:1673-1681.
8. Isla H, Srebro-Hooper M, Jean M, Vanthuyne N, Roisnel T, Lunkley JL, Muller G, Williams JAG, Autschbach J, Crassous J. Conformational changes and chiroptical switching of enantiopure bis-helicenic terpyridine upon Zn^{2+} binding. *Chem Commun*. 2016;52:5932-5935.
9. Chelucci G, Thummel RP. Chiral 2,2'-Bipyridines, 1,10-Phenanthrolines, and 2,2':6',2'' -Terpyridines: Syntheses and Applications in Asymmetric Homogeneous Catalysis. *Chem. Rev.* 2002;102:3129-3170
10. Kwong H-L, Yeung H-L, Yeung C-T, Lee W-S, Lee C-S, Wong W-L. Chiral pyridine-containing ligands in asymmetric catalysis. *Coord Chem Rev*. 2007;251:2188-2222.
11. Cortijo M, Viala C, Reynaldo T, Favereau L, Fabing I, Srebro-Hooper M, Autschbach J, Ratel-Ramond N, Crassous J, Bonvoisin J. Synthesis, spectroelectrochemical behavior, and chiroptical switching of tris(β-diketonato) complexes of ruthenium(III), chromium(III), and cobalt(III). *Inorg Chem.* 2017;56:4555-4567.
12. Das A, Ghosh P, Plebst S, Schwederski B, Mobin SM, Kaim W, Lahiri GK. Ancillary Ligand Control of Electronic Structure in o-Benzoquinonediimine-Ruthenium Complex Redox Series: Structures, Electron Paramagnetic Resonance (EPR), and Ultraviolet-Visible-Near-Infrared (UV-vis-NIR) Spectroelectrochemistry. *Inorg Chem.* 2015;54: 3376-3386
13. Mondal P, Das A, Lahiri GK. The Electron-Rich {$Ru(acac)_2$} Directed Varying Configuration of the Deprotonated Indigo and Evidence for Its Bidirectional Non-innocence. *Inorg Chem*. **2016**;55:1208-1218.
14. Grupp A, Bubrin M, Ehret F, Zeng Q, Hartl F, Kvapilova H, Zalis S, Kaim W. Ru-^{II}(α-diimine) or Ru-^{III}(α-diimine$^{\bullet-}$)? Structural, Spectroscopic, and Theoretical Evidence for the Stabilization of a Prominent Metal-to-Ligand Charge-Transfer Excited-State Configuration in the Ground State. *Eur J Inorg Chem.* 2014;110-119.
15. Kasahara, Y, Hoshino, Y, Shimizu, K, Sato, GP. Reaction of tris(β-diketonato)ruthenium(III) complexes with strong acids in acetonitrile. Formation of bis(acetonitrile)bis(β-diketonato)ruthenium(III) complexes. Chemistry Lett. 1990;3:381-4.
16. Saleh N, Srebro M, Reynaldo T, Vanthuyne N, Toupet L, Chang VY, Muller G, Williams JAG, Roussel C, Autschbach J, Crassous, J. Enantio-enriched CPL-active helicene-bipyridine-rhenium complexes. *Chem. Comm.* 2015;51:3754-3757.
17. Ou-Yang J-K, Saleh N, Fernandez Garcia G, Norel L, Pointillart F, Guizouarn T, Cador O, Totti F, Ouahab L, Crassous J, Le Guennic B. *Chem. Comm.* 2016;52:14474-14477.
18. TURBOMOLE V6.6 2014, a development of University of Karlsruhe and Forschungszentrum Karlsruhe GmbH, 1989-2007, TURBOMOLE GmbH, since 2007; available from http://www.turbomole.com.
19. Ahlrichs R, Bär M, Häser M, Horn H, Kölmel C. Electronic structure calculations on workstation computers: the program system turbomole. *Chem Phys Lett*. **1989**;162:165-169.
20. Furche F, Ahlrichs R, Hättig C, Klopper W, Sierka M, Weigend F. Turbomole. *WIREs Comput Mol Sci*. 2014;4:91-100.
21. Srebro-Hooper M, Autschbach J. Calculating natural optical activity of molecules from first principles. *Annu Rev Phys Chem*. 2017;68:399-420.
22. Autschbach J. Computing chiroptical properties with first–principles theoretical methods: Background and illustrative examples, *Chirality* 2009:21:E116–E152.
23. Becke AD. Density-functional exchange-energy approximation with correct asymptotic behavior. *Phys Rev A*. 1988;38:3098-3100.
24. Perdew JP. Density-functional approximation for the correlation energy of the inhomogeneous electron gas. *Phys Rev B*. 1986;33:8822-8824.

25. Perdew JP. Erratum: density-functional approximation for the correlation energy of the inhomogeneous electron gas. *Phys Rev B*. 1986;34:7406.

26. Lee CT, Yang WT, Parr RG. Development of the Colle-Salvetti correlation-energy formula into a functional of the electron density. *Phys Rev B*. 1988;37:785-789.

27. Becke AD. Density functional thermochemistry. III. The role of exact exchange. *J Chem Phys*. 1993;98:5648-5652

28. Stephens PJ, Devlin FJ, Chabalowski CF, Frisch MJ. Ab initio calculation of vibrational absorption and circular dichroism spectra using density functional force fields. *J Phys Chem*. 1994;98:11623-11627.

29. Adamo C, Barone V. Toward reliable density functional methods without adjustable parameters: The PBE0 model. *J Chem Phys*. 1999;110:6158-6170.

30. Becke AD. A new mixing of Hartree-Fock and local density–functional theories. *J Chem Phys*. 1993; 98:1372-1377.

31. Schäfer A, Horn H, Ahlrichs R. Fully optimized contracted Gaussian basis sets for atoms Li to Kr. *J Chem Phys*. 1992;97:2571-2577.

32. Eichkorn K, Weigend F, Treutler O, Ahlrichs R. Auxiliary basis sets for main row atoms and transition metals and their use to approximate Coulomb potentials. *Theor Chem Acc*. 1997;97:119-124.

33. Weigend F, Ahlrichs R. Balanced basis sets of split valence, triple zeta valence and quadruple zeta valence quality for H to Rn: design and assessment of accuracy. *Phys Chem Chem Phys*. 2005;7:3297-3305.

34. Andrae D, Haussermann U, Dolg M, Stoll H, Preuss H. Energy-adjusted ab initio pseudopotentials for the second and third row transition elements. *Theoret Chim Acta*. 1990;77:123-141.

35. Klamt A, Schüürmann GJ. COSMO: a new approach to dielectric screening in solvents with explicit expressions for the screening energy and its gradient. *J Chem Soc, Perkin Trans 2*. 1993:799-805.

36. Klamt A. Calculation of UV/Vis spectra in solution. *J Phys Chem*. 1996;100:3349-3353.

37. Autschbach J, Ziegler T, van Gisbergen SJA, Baerends EJ. Chiroptical properties from time-dependent density functional theory. I. Circular dichroism spectra of organic molecules. *J Chem Phys*. 2002;116:6930-6940.

38. Lashdaf M, Hatanpää T, Tiitta M. Volatile β-diketonato complexes of ruthenium, palladium and platinum. *Journal of Thermal Analysis and Calorimetry* 2001;64:1171-1182.

39. Lee DJ, Kang S-W, Rhee S-W. Chemical vapor deposition of ruthenium oxide thin films from $Ru(tmhd)_3$ using direct liquid injection. *Thin Solid Films* 2002;413:237-242.

40. Autschbach J., Srebro M. Delocalization Error and "Functional Tuning" in Kohn–Sham Calculations of Molecular Properties. *Acc Chem Res*. 2014;47:2592-2602.